

Supplementary information

Three-Dimensional Bowl-Shaped Solid Additive Achieves 20.52% Efficiency Organic Solar Cells with Enhanced Thermal Stability via Curvature-Mediated Morphology Regulation†

Zhicheng Zhong,^{‡a} Sergio Gámez-Valenzuela,^{‡a} Jin-Woo Lee,^b Yufei Wang,^c Bolin Li,^a Guanshui Xie,^d Weijie Zhou,^a Changjing Xu,^a Dingqin Hu,^a Haihui Cai,^a Qing Lian,^a Longbin Qiu,^d Guangye Zhang,^c Mingwei An*,^{a,e} Yang Wang,^e Bumjoon J. Kim,^b Xugang Guo*,^a and Bin Liu*^a

^a Department of Materials Science and Engineering, Southern University of Science and Technology (SUSTech), Shenzhen, Guangdong 518055, P. R. China
E-mail: guoxg@sustech.edu.cn, liub3@sustech.edu.cn

^b Department of Chemical and Biomolecular Engineering, Korea Advanced Institute of Science and Technology (KAIST), Daejeon 34141, Republic of Korea

^c College of New Materials and New Energies, Shenzhen Technology University, Shenzhen, Guangdong 518118, P. R. China

^d Department of Mechanical and Energy Engineering, SUSTech Energy Institute for Carbon Neutrality, Southern University of Science and Technology (SUSTech), Shenzhen, Guangdong 518055, P. R. China

^e Strait Institute of Flexible Electronics (SIFEFuture Technologies), Fujian Key Laboratory of Flexible Electronics, Fujian Normal University and Strait Laboratory of Flexible Electronics (SLoFE), Fuzhou, Fujian 350117, P. R. China
E-mail: ifemwan@fjnu.edu.cn

[‡]These authors contributed equally to this work.

[†]Electronic supplementary information (ESI) available.

Table of Contents

1. Supplementary Experiment Procedures
2. Supplementary Figures
3. Supplementary Tables
4. Supplementary References

1. Supplementary Experiment Procedures

Materials. Corannulene (C_2H_{10}) is a bowl-shaped polycyclic aromatic hydrocarbon composed of a central five-membered ring fused with five benzene rings, forming a curved, non-planar structure resembling a fragment of a fullerene (like C_{60}). Corannulene does not occur naturally in usable quantities and must be obtained through laboratory synthesis or commercial suppliers. In this study, corannulene was synthesized *via* an eight-step route starting from 2,7-dihydroxynaphthalene, a commercially available raw material (purchased from Energy Chemical Co., Ltd), as shown in **Fig. S1**. The total overall yield of the synthesis was 17.4%, which is consistent with literature-reported values for polycyclic aromatic systems of similar complexity.

The donor polymer PM6 and the non-fullerene acceptor L8-BO were both purchased from Solarmer Beijing Inc. PM6 exhibits HOMO and LOMO energy levels of -5.49 eV and -3.01 eV, respectively, while L8-BO possesses energy levels of -5.67 eV (HOMO) and -3.97 eV (LUMO). The hole transport layer material PEDOT:PSS (Clevios P VP A1 4083), with a work function of approximately 5.0 eV, was obtained from eFlexPV, with a concentration of 1.5 wt% soluble in water. Unless otherwise stated, all chemicals and agents were obtained from commercial sources and used without further purification. Anhydrous toluene was distilled from Na/benzophenone under an argon flow.

TGA. Thermogravimetric analysis (TGA) of the solid additives corannulene and coronene was conducted using a HITACHI STA200 simultaneous thermal analyzer. The measurements were performed on the bulk materials at a scanning rate of 10°C/min, starting from ambient temperature and increasing up to 300°C. The temperature was maintained at 100°C throughout the heating cycle for 1 hour.

UV-vis absorption spectra. UV-vis absorption spectra of PM6:L8-BO blend films, without or with different additives, were acquired using a Shimadzu UV-3600 UV-VIS-NIR spectrophotometer.

DFT calculations. The molecular geometries of isolated species, including a monomeric model of the PM6 polymer, the L8-BO acceptor, and each additive, were optimized at the Density Functional Theory (DFT) level using the GAUSSIAN16 program.¹ The hybrid generalized gradient approximation (GGA) functional B3LYP² was employed in combination with the 6-31G** basis set. These calculations were performed in the gas phase and serve to evaluate key intrinsic properties of the molecules, such as dipole moment, electrostatic potential distribution, and frontier orbital energies, which are relevant for understanding their interaction tendencies and miscibility in blend films. To reduce computational cost without significantly affecting the electronic structure of the core, all long alkyl side chains were replaced with methyl groups in these calculations.

To further investigate the nature of molecular interactions between additives and the donor or acceptor components, representative bimolecular complexes were constructed. These included one molecule of additive and either a dimeric segment of PM6 or a single L8-BO molecule. Prior to DFT optimization, a conformational pre-screening was carried out using Molecular Mechanics (MM) with the Avogadro software, which offers useful capabilities for comprehensive exploration of low-energy conformers in molecular clusters.^{3–6} The most stable conformations were then optimized at the B3LYP-D3/6-31G** level of theory, which incorporates an empirical D3 dispersion correction to account for long-range van der Waals interactions.⁷ The resulting geometries, illustrated in Figures S3 and S4, consider interactions between additives and the different moieties of the PM6 and L8-BO systems, including both concave and convex orientations of the corannulene molecule. It is important to note that these gas-phase calculations do not explicitly model the annealed or bulk-processed film morphologies, but serve as a first-principles approach to reveal fundamental interaction trends and thermodynamic preferences that typically help rationalize experimental observations of morphology, phase behavior, and performance. Frequency calculations were computed at the same level of theory to derive Gibbs free energies at 298.15 K. No imaginary frequencies were observed. The Gibbs free energies of formation were calculated by the equation $\Delta G^{\circ f} = G_{\text{Com}} - (G_{M1} + G_{M2})$, where G_{Com} is the Gibbs free energy of the complex, and G_{M1} and G_{M2} are the Gibbs free energies of the interacting molecules. On the other hand, bonding energies (E_{bonding}) were calculated as the

difference between the total energies of the complexes and the optimized corresponding interacting molecules.⁸ Interaction energies ($E_{\text{interaction}}$) were calculated as the difference between the total energies of the complexes and the energies of the interacting molecules in the conformation that they adopt to form the complex. Finally, reorganization energies ($E_{\text{reorganization}}$) were calculated as the difference between E_{bonding} and $E_{\text{interaction}}$.

Contact angle measurement. Contact angles were recorded using an SDC-200S contact angle goniometer, employing water and ethylene glycol (EG) as test fluids.

Device fabrication. Conventional-structured OSCs were fabricated using the following configuration: ITO/PEDOT:PSS/Active Layer/PNDIT-F3N/Ag. The effective area of the OSC devices is 0.064 cm² (the region where the ITO electrode and Ag electrode overlap). The substrates utilized were pre-patterned ITO-coated glasses with a sheet resistance of 15 Ω sq⁻¹, which were cleaned sequentially by sonication in detergent-infused water, deionized water, acetone, and isopropanol, followed by drying in a vacuum oven. A final UV-ozone treatment was performed for 15 min using a BZS250GF-TC UV-ozone (HWOTECH) system. The PEDOT:PSS layers were spin-coated onto the UV-ozone-treated ITO substrates at a speed of 5000 rpm for 20 s. Following this, the coated substrates were annealed at 150 °C for 10 min under ambient conditions before being transferred into a glove box for further processing. For PM6:L8-BO-based devices, the active layer solution was prepared with a polymer concentration of 7.2 mg mL⁻¹ (donor: acceptor = 1:1.25, w/w) and spin-coated onto the substrates. In control devices, 1,8-diiodooctane (DIO) (0.25%, v/v) was used as the solvent additive. For PM6:L8-BO based devices incorporating solid additives, corannulene or coronene (15%, w/w, relative to the donor) were added. The samples were then thermally annealed at 65 °C for 8 min. The photoactive layer, with an ideal thickness of ~110 nm, was prepared on the PEDOT: PSS layer and then placed at room temperature for 10 min. Subsequently, PNDIT-F3N dissolved in methanol at a concentration of 0.5 mg mL⁻¹ with 0.5 vt.% acetic acid was spin-deposited onto the active layers at a speed of 2000 rpm for 30 s. Finally, a layer of Ag with a thickness of 110 nm was coated onto the electron transport layer via thermal evaporation under high vacuum (ca. 1×10^{-6} Pa).

Device characterization. The current-voltage (J - V) characteristics of all devices were measured under simulated AM1.5G illumination (100 mW cm⁻²) using an SS-F5-3A Solar Simulator (Enli Technology, Inc.) equipped with a xenon (Xe) lamp. The white light source consisted of an Xe lamp with an AM1.5G filter, and the light intensity was calibrated using a Si solar cell, which was standardized by the National Renewable Energy Laboratory (NREL). The reference silicon solar cell we used for calibration has a quartz window, which does not filter out the spectrum beyond 900 nm. The EQE curves were determined using a QE-R3011 measurement system from Enli Technology, Inc.

SCLC measurement. Charge carrier mobilities were assessed using the space-charge-limited current (SCLC) method. For hole-only devices, the device structure was ITO/PEDOT:PSS/active layer/MoO₃/Ag, while for electron-only devices, the structure was ITO/ZnO/active layer/Ca/Al. The mobilities were calculated using the Mott-

Gurney equation:
$$J = \frac{9}{8} \varepsilon_r \varepsilon_0 \mu \frac{V^2}{L^3}$$
, where J is the current density, ε_r is the relative permittivity of the photoactive material (typically 2 to 4 for organic/polymer semiconductors, and assumed to be 3 for polymers in this study), ε_0 is the permittivity of free space, μ is the mobility of holes or electrons, L is the active layer thickness, and V is the internal voltage, defined as $V = V_{\text{appl}} - V_{\text{bi}}$. Here, V_{appl} is the applied voltage, and V_{bi} is the built-in voltage, which is the difference in work function between the two electrodes. In electron-only and hole-only devices, V_{bi} can be neglected.

Transient photovoltage (TPV) and transient photocurrent (TPC) measurements

During TPV evaluations, devices were illuminated under ambient conditions using a Quartz Tungsten-Halogen Lamp. The light intensity was adjusted to match the operational conditions of the devices, thereby ensuring their voltage aligned with the V_{oc} under solar simulation. Photo-excitation was induced using 8 ns pulsed laser emissions from the NLD520 system (Oriental Spectra) with the excitation wavelength precisely set at 518 nm and a narrow spectral bandwidth of 3 nm. The TPV responses

were captured under open-circuit conditions using a high-resolution digital oscilloscope. Concurrently, TPC measurements were conducted under short-circuit conditions, employing identical excitation parameters but in the absence of background illumination.

Femtosecond time-resolved Transient Absorption Spectroscopy (fs-TAS)

Measurements. Femtosecond transient absorption (fs-TA) spectroscopy was employed to track the absorption changes in excited states over time, thereby elucidating the carrier dynamics on the femtosecond to nanosecond scale. The excitation source was an amplified Yb laser (1046 nm) that produced 283.9 fs pulses at a 2 kHz repetition rate. The laser power is 500 μ J, and the spectral range used is 480~950 nm. The output was divided into two beams; the more intense one served as the 1046 nm pump light, while the other was directed into a sapphire plate to create a broadband supercontinuum probe light. An optical chopper was used to adjust the pump pulses' repetition rate to 500 Hz, which were then focused on the sample in conjunction with the probe pulse (white light). The TA spectra were derived by comparing the probe light spectra with and without the pump light excitation. The photoinduced changes in absorption as a function of wavelength were represented in terms of optical density (OD) changes ($\Delta OD(\lambda)$). By fine-tuning the delay between the pump and probe pulses, a 3D transient spectral image $\Delta OD (\lambda,t)$ was constructed.

Energy loss analysis

According to the Shockley-Queisser (SQ) limit theory, energy losses are typically categorized into three parts: radiative losses above the optical bandgap (ΔE_1), radiative losses below the optical bandgap (ΔE_2), and non-radiative recombination losses (ΔE_3). The quantitative expressions for these energy losses can be formulated as:

$$\begin{aligned} E_{\text{loss}} &= E_g - qV_{\text{oc}} \\ &= (E_g - qV_{\text{oc}}^{\text{SQ}}) + (q\Delta V_{\text{oc}}^{\text{rad,below gap}}) + (q\Delta V_{\text{oc}}^{\text{non-rad}}) \\ &= \Delta E_1 + \Delta E_2 + \Delta E_3 \end{aligned}$$

V_{oc}^{SQ} is the maximum open-circuit voltage calculated according to the SQ theory, $\Delta V_{oc}^{rad\ below\ gap}$ denotes the radiative recombination open-circuit voltage loss below the optical bandgap, and $\Delta V_{oc}^{non-rad}$ signifies the non-radiative recombination open-circuit voltage loss.

The SQ limit open-circuit voltage can be expressed as:

$$V_{oc}^{SQ} = \frac{kT}{q} \ln \left(\frac{J_{sc}}{J_0^{SQ}} + 1 \right) = \frac{kT}{q} \ln \left(\frac{q \cdot \int_0^{\infty} EQE_{PV}(E) \cdot \phi_{AM1.5}(E) dE}{q \cdot \int_{E_{gap}}^{\infty} \phi_{BB}(E) dE} \right) + 1$$

The voltage loss below the optical bandgap ($\Delta V_{oc}^{rad\ below\ gap}$) can be calculated using Equation below:

$$\Delta V_{oc}^{rad\ below\ gap} = V_{oc}^{SQ} - V_{oc}^{rad}$$

The non-radiative voltage loss ($\Delta V_{oc}^{non-rad}$) can be calculated using the following formula:

$$\Delta V_{oc}^{non-rad} = V_{oc}^{rad} - V_{oc}$$

ΔV_{oc}^{rad} is the open-circuit voltage due to radiative recombination, and V_{oc} is the open-circuit voltage measured through *I-V* testing of the solar cell.

The formula can also be expressed as:

$$V_{oc}^{non-rad} = -\frac{kT}{q} \ln (EQE_{EL})$$

AFM. The film morphology of the active layers containing solid additives was analyzed using Atomic Force Microscopy (AFM). The measurements were conducted in tapping mode with a Dimension Icon Scanning Probe Microscope (Asylum Research, MFP-3D-Stand Alone).

TEM. Transmission electron microscopy (TEM) images were acquired using a Hitachi HT7700 microscope running at 100 kV and outfitted with an AMF-5016 charge-coupled device (CCD) detector.

GIWAXS measurements. GIWAXS measurements were executed at the PLS-II 9A U-SAXS (Ultra-Small-Angle X-ray Scattering) beamline of the Pohang Accelerator Laboratory in Republic of Korea.

2. Supplementary Figures

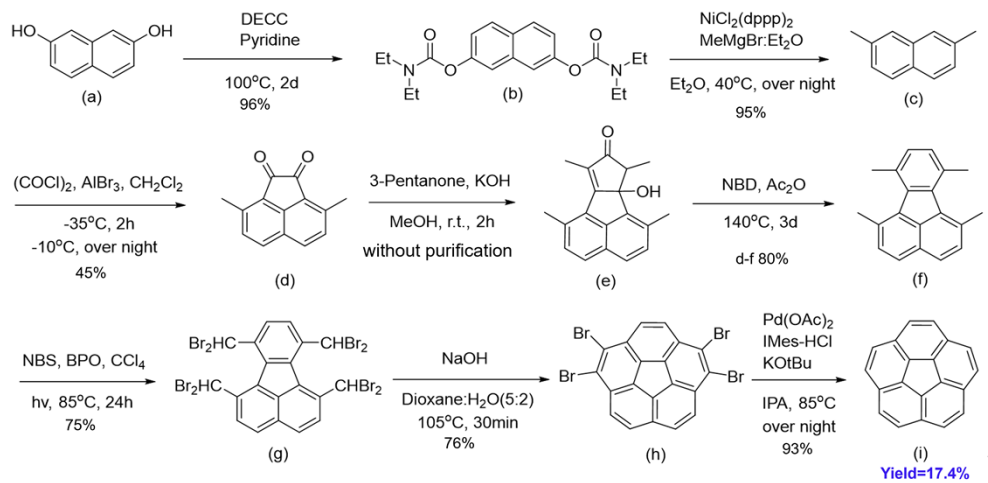


Fig. S1 The synthetic route of corannulene.

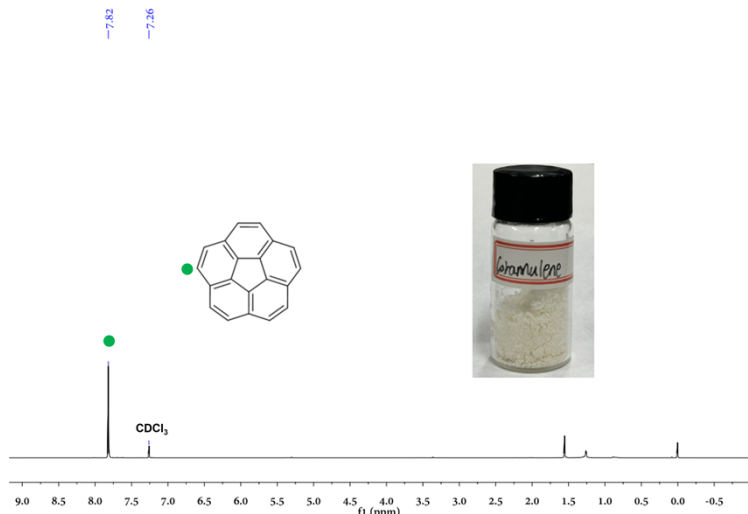


Fig. S2 ¹H NMR spectrum of corannulene (400 MHz, CDCl₃). The inset depicts corannulene as a light-yellow powder.

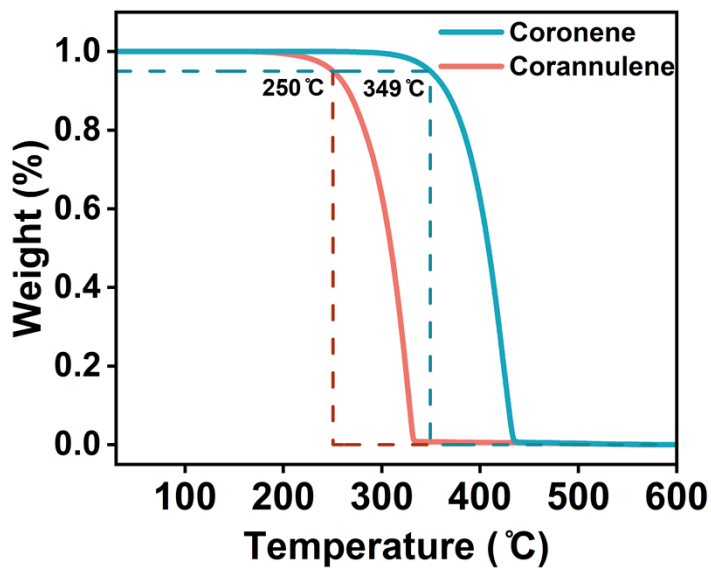


Fig. S3 TGA plots of coronene and corannulene obtained under an inert nitrogen atmosphere at a scan rate of $10\text{ }^{\circ}\text{C min}^{-1}$.

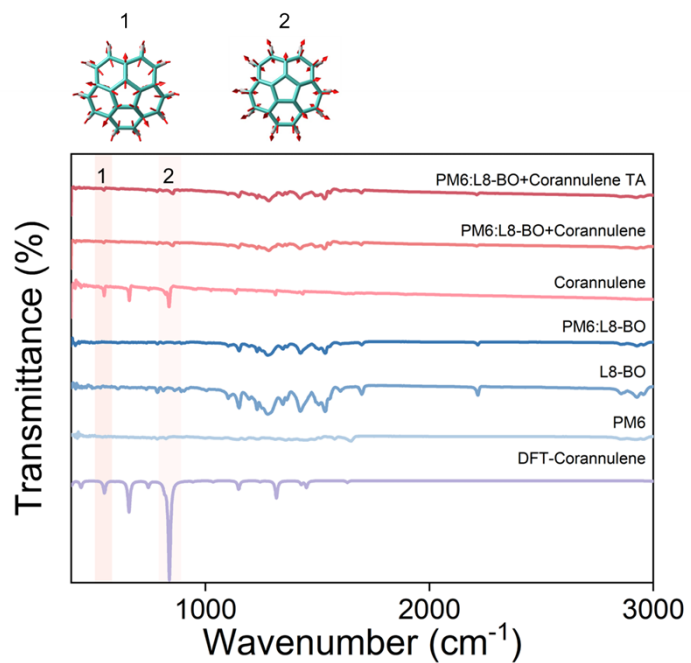


Fig. S4 FT-IR spectra of PM6, L8-BO, corannulene, DFT-calculated corannulene, and corannulene-treated PM6:L8-BO systems before and after thermal annealing. The vibrational eigenvectors associated with the highlighted peaks are also shown.

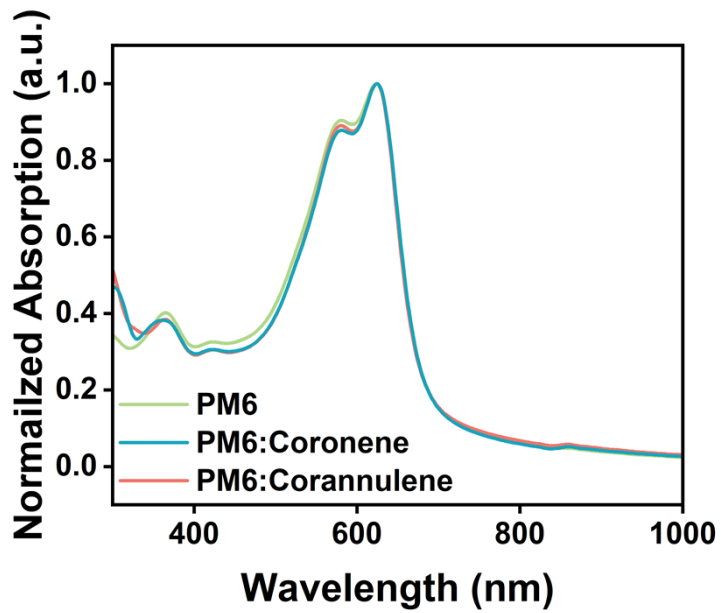


Fig. S5 UV–vis absorption spectra of PM6, PM6:Coronene, and PM6:Corannulene films.

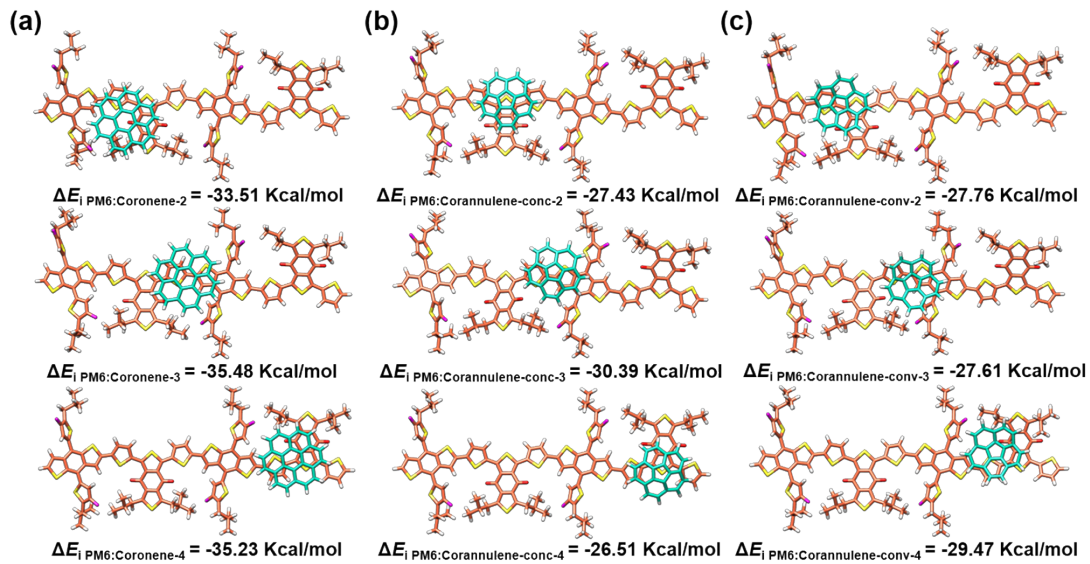


Fig. S6 DFT-optimized conformations and calculated interaction energies for the molecular complexes of (a) PM6:Coronene, (b) PM6:Corannulene-concave, and (c) PM6:Corannulene-convex.

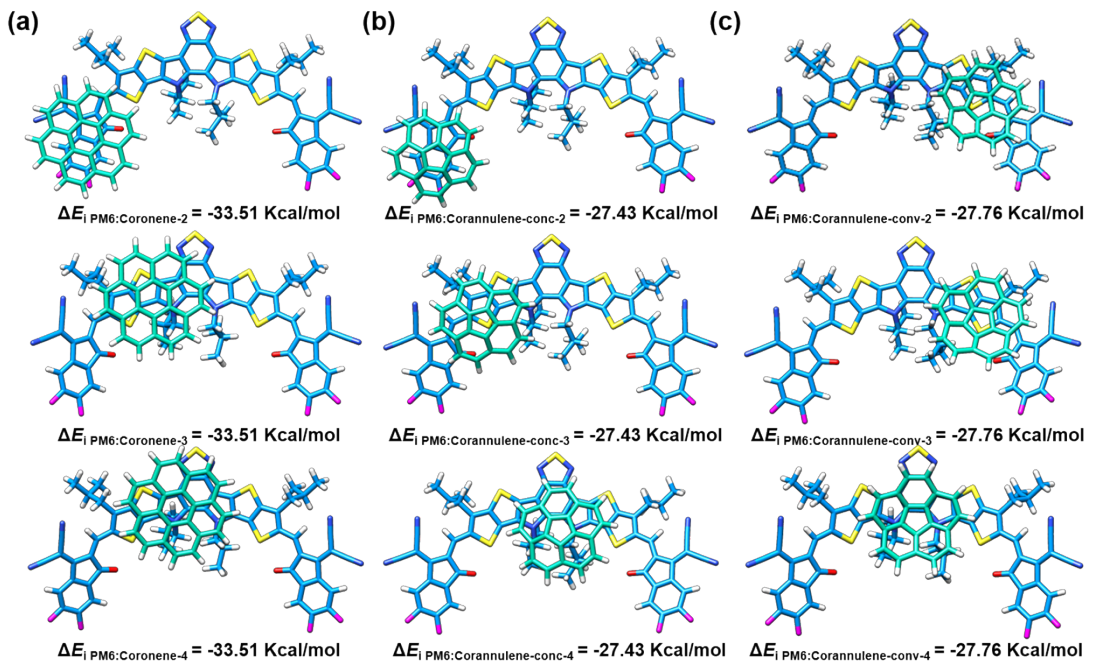


Fig. S7 DFT-optimized conformations and calculated interaction energies for the molecular complexes of (a) L8-BO:Coronene, (b) L8-BO:Corannulene-concave, and (c) L8-BO:Corannulene-convex.

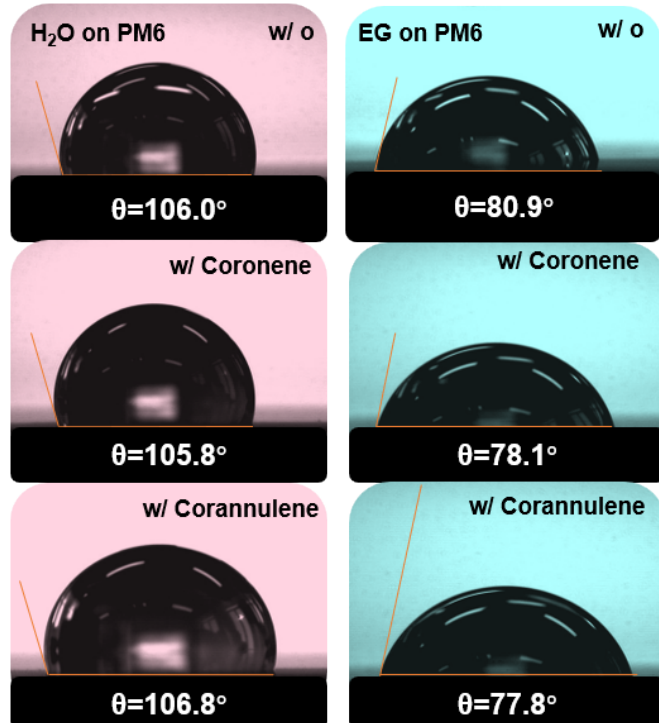


Fig. S8 Contact angles of bare PM6, PM6:Corannulene and PM6:Coronene substrates, measured by applying deionized water liquid (left) an dethylene glycol drops (right).

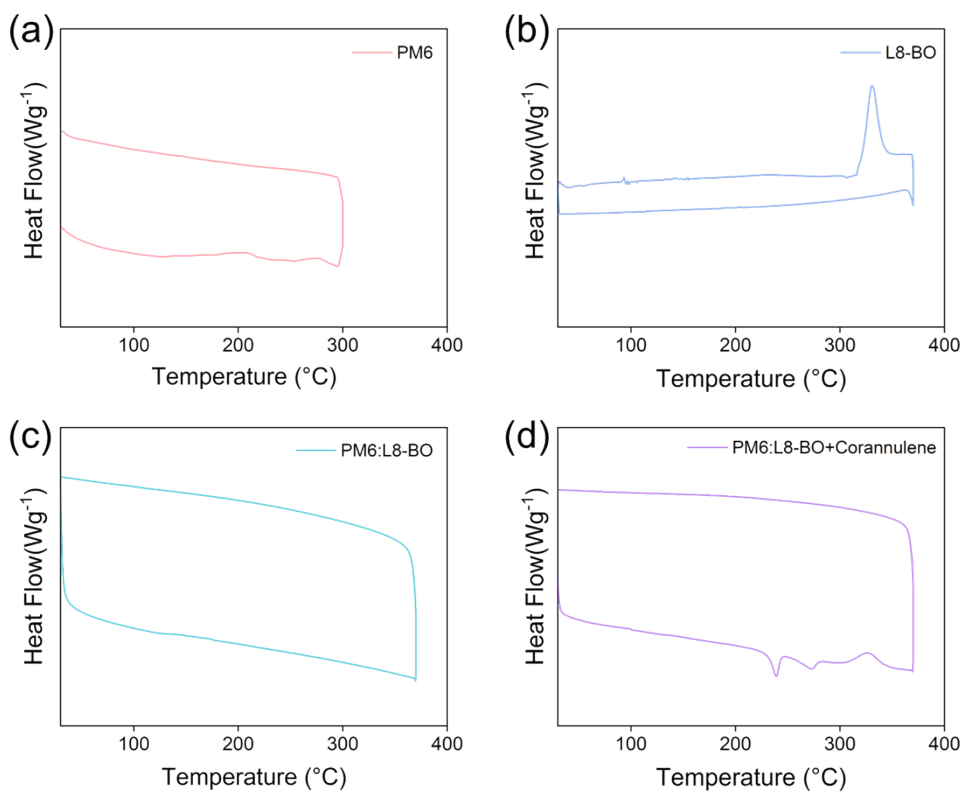


Fig. S9 DSC curves of PM6, L8-BO, PM6:L8-BO and PM6:L8-BO with corannulene.

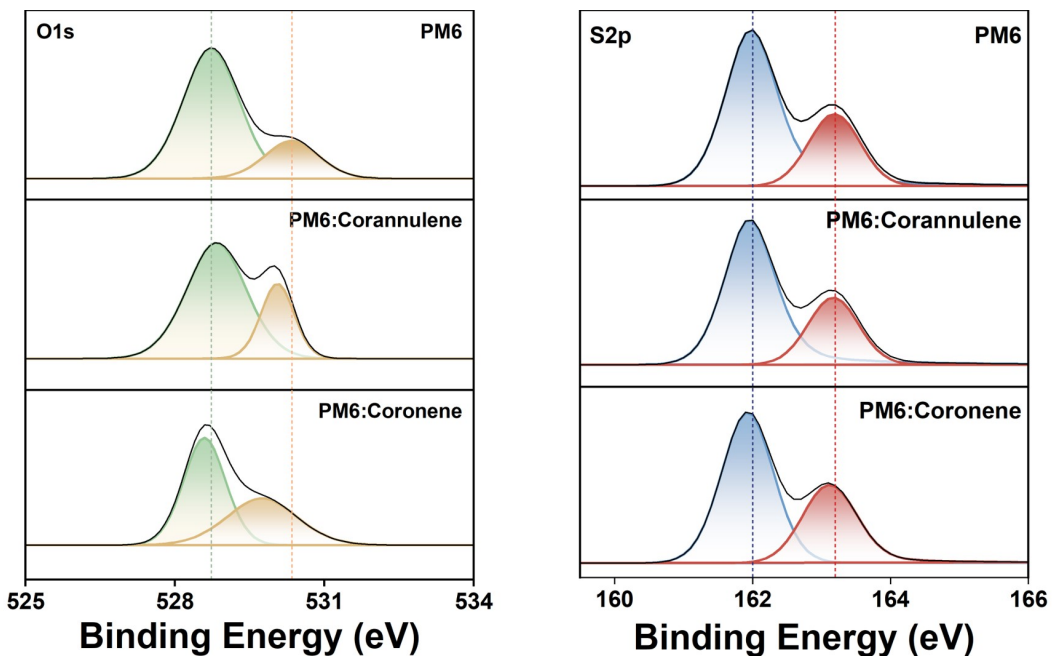


Fig. S10 O 1s (left) and S 2p (right) XPS spectra of PM6, PM6:Corannulene, and PM6:Coronene systems after annealing.

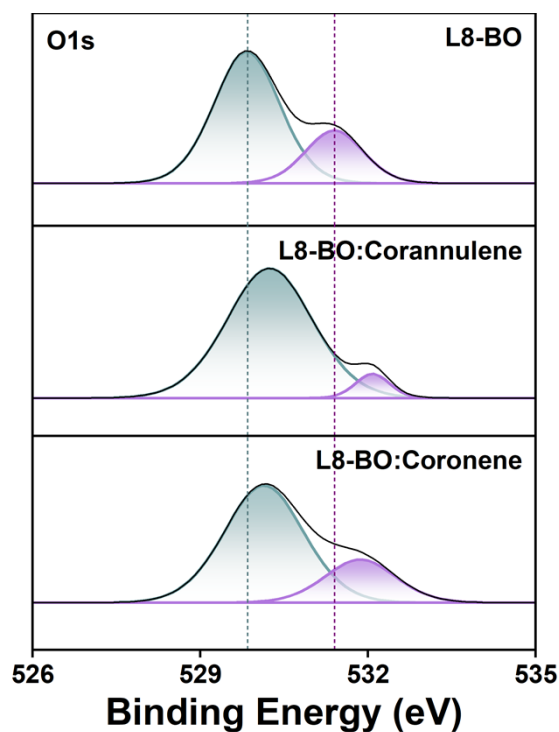


Fig. S11 O 1s XPS spectra of L8-BO, L8-BO:Corannulene, and L8-BO:Coronene systems after annealing.



华南国家计量测试中心
广东省计量科学研究院
SOUTH CHINA NATIONAL CENTER OF METROLOGY
GUANGDONG INSTITUTE OF METROLOGY

校准证书
CALIBRATION CERTIFICATE

证书编号 NYX202500019
Certificate No.

第 1 页, 共 5 页
Page 1 of 5

客户名称 Name of the Customer	南方科技大学 Southern University of Science and Technology
联络信息 Contact Information	广东省深圳市南山区学苑大道1088号 No.1088 Xueyuan Avenue, Nanshan District, Shenzhen, Guangdong
计量器具名称 Description	有机太阳能电池 Organic solar cells
型号/规格 Model/Type	有机太阳能电池 Organic solar cells
制造厂 Manufacturer	南方科技大学郭旭岗教授课题组 Prof. Xugang Guo's Group from Southern University of Science and Technology
出厂编号 Serial No.	G-OSC-3
接收日期 Receipt on	2025 年 01 月 15 日 Y M D

结论 Conclusion	见校准结果 Shown in the results of calibration
校准日期 Calibration on	2025 年 01 月 15 日 Y M D
发布日期 Issue on	2025 年 01 月 22 日 Y M D

批 准 Authorized by	周军红 周军红
核 验 Reviewed by	林鼎添 林鼎添
校 准 Calibrated by	梅书刚 梅书刚



扫一扫查真伪

实验室地址: 广东省东莞市石排镇东园大道石排段152号 邮政编码: 523343
电话: (8620)86594172 传真: (8620)86590743 投诉电话: (8620)36611242 E-mail: scm@scm.com.cn
Add: No.1, Miaobianwang Section, Dongyuan Road South, Shipai Town, Dongguan, Guangdong.
Post Code: 523343 Tel: (8620)86594172 Fax: (8620)86590743 Complaint Tel: (8620)36611242
证书真伪查询: www.scm.com.cn; cert.scm.com.cn Certificate Authenticity Identify: www.scm.com.cn; cert.scm.com.cn

5250117006 2


华南国家计量测试中心
广东省计量科学研究院
SOUTH CHINA NATIONAL CENTER OF METROLOGY
GUANGDONG INSTITUTE OF METROLOGY

校准结果

RESULTS OF CALIBRATION

证书编号 NYX202500019
 Certificate No.

原始记录号 NYX202500019
 Record No.

第 4 页, 共 5 页
 Page 4 of

1、外观检查: 符合要求
 Apparent Inspection: Pass.

2、测试条件: 温度(25 ± 2) $^{\circ}\text{C}$; 辐照度 1000W/m^2 .
 Test conditions: Temperature: (25 ± 2) $^{\circ}\text{C}$; Irradiance: 1000W/m^2 .

3、电流-电压特性曲线和功率-电压特性曲线:
 I-V and P-V curves:

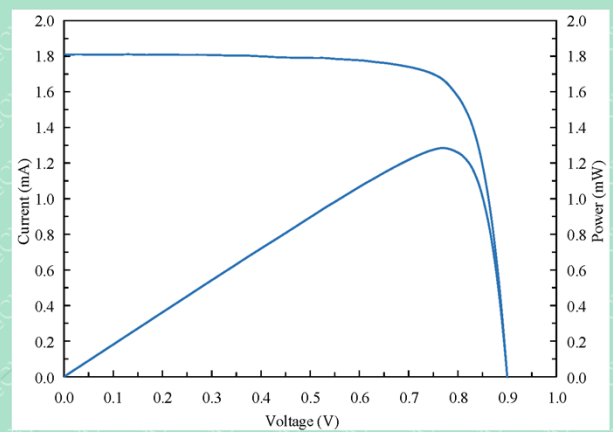


图1 电流-电压特性曲线和功率-电压特性曲线

Figure1 I-V and P-V characteristic curves

4、光电性能参数:

Results of photoelectric properties:

表1(Table 1)

面积	短路电流密度 J_{sc}	短路电流 I_{sc}	开路电压 V_{oc}	填充因子 FF	最大功率 P_m	最佳工作电流 I_m	最佳工作电压 V_m	转换效率 η
Area	Short circuit current density	Short circuit current	Open circuit voltage	Fill factor	Maximum power	Optimum working current	Optimum working voltage	Efficiency
cm ²	mA/cm ²	mA	V	%	mW	mA	V	%
0.0647	27.98	1.810	0.899	78.90	1.284	1.668	0.770	19.85

Fig. S12 The certification report of PM6:L8-BO-based device processed with corannulene, provided by the South China National Center of Metrology.

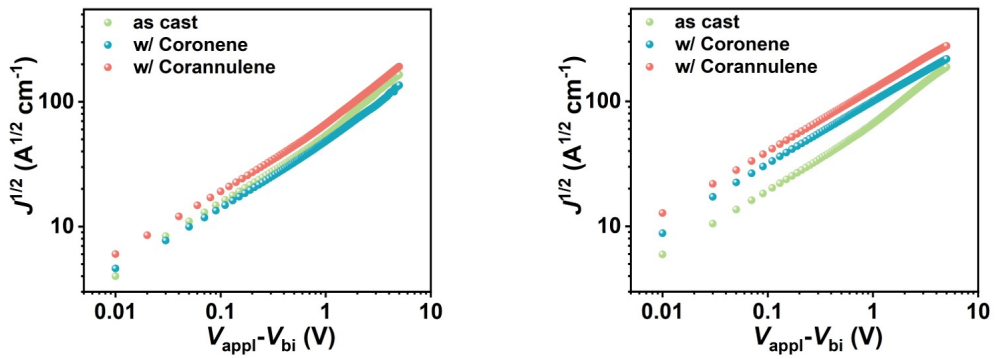


Fig. S13 J - V curves of the (a) hole-only and (b) electron-only devices with the optimal active layer under dark conditions.

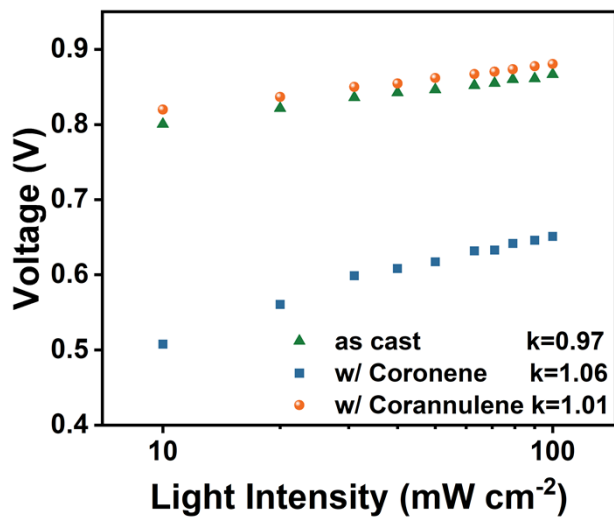


Fig. S14 Dependences of V_{oc} on P_{light} for OSCs.

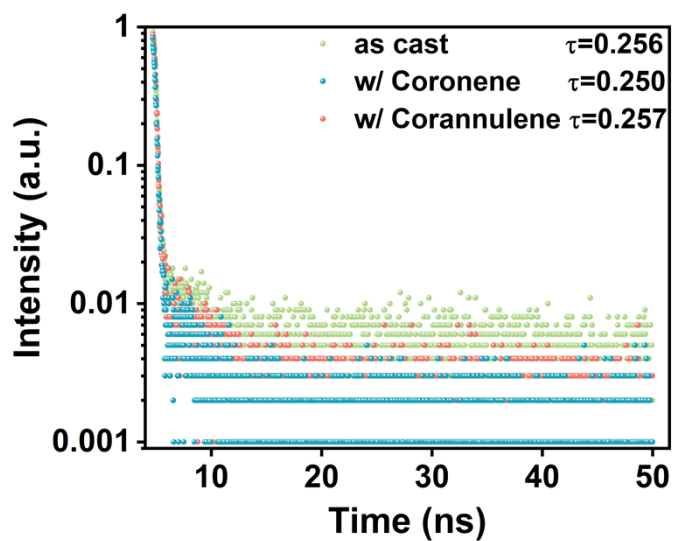


Fig. S15 TRPL spectra of the blend films.

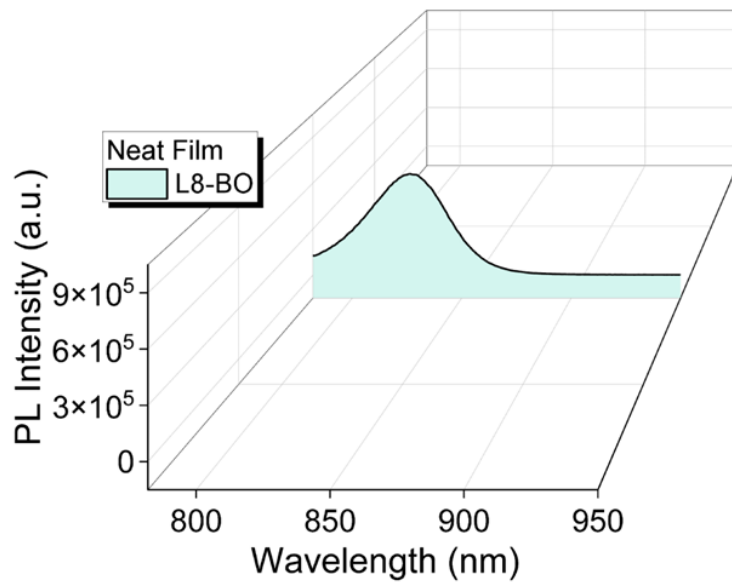


Fig. S16 PL spectrum of the neat L8-BO film under 780 nm excitation.

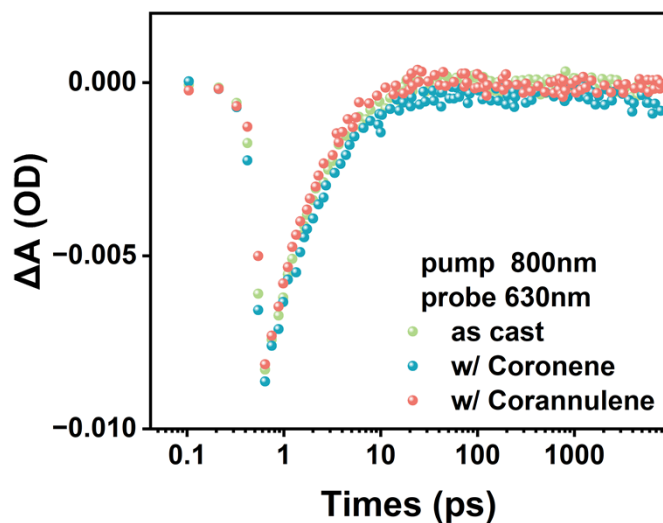


Fig. S17 Comparison of the hole-transfer kinetics for the corresponding blend films.

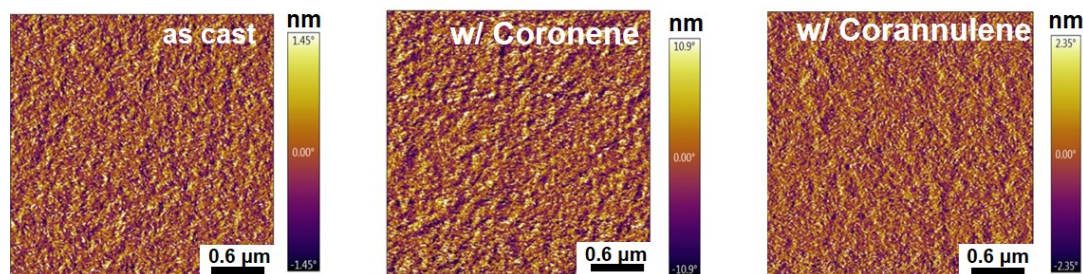


Fig. S18 AFM phase images of PM6:L8-BO blend films with various solid additives.

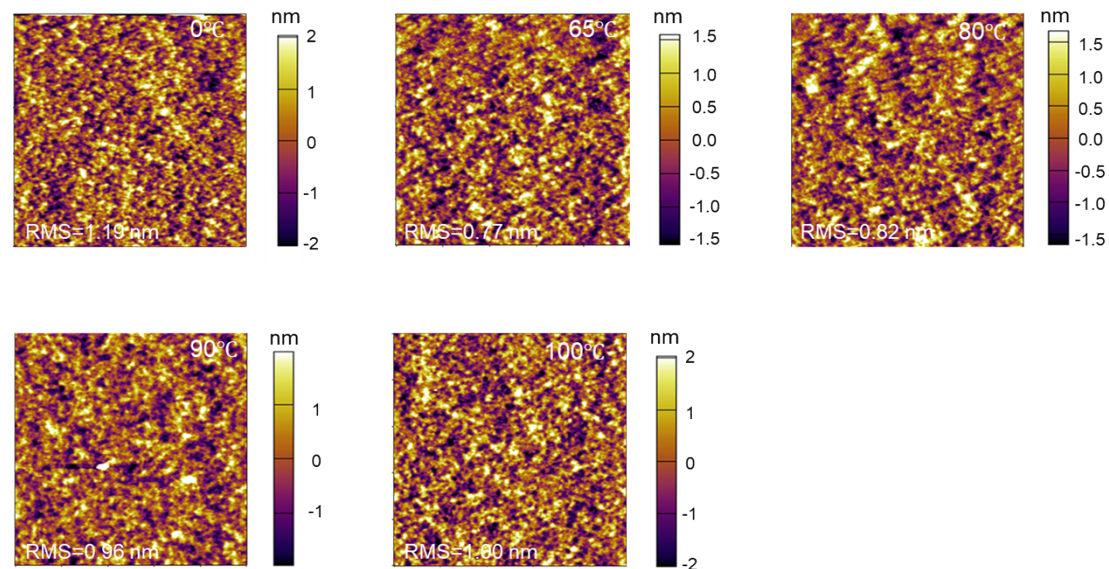


Fig. S19 AFM height images of PM6:L8-BO blend films treated with corannulene under different thermal annealing conditions.

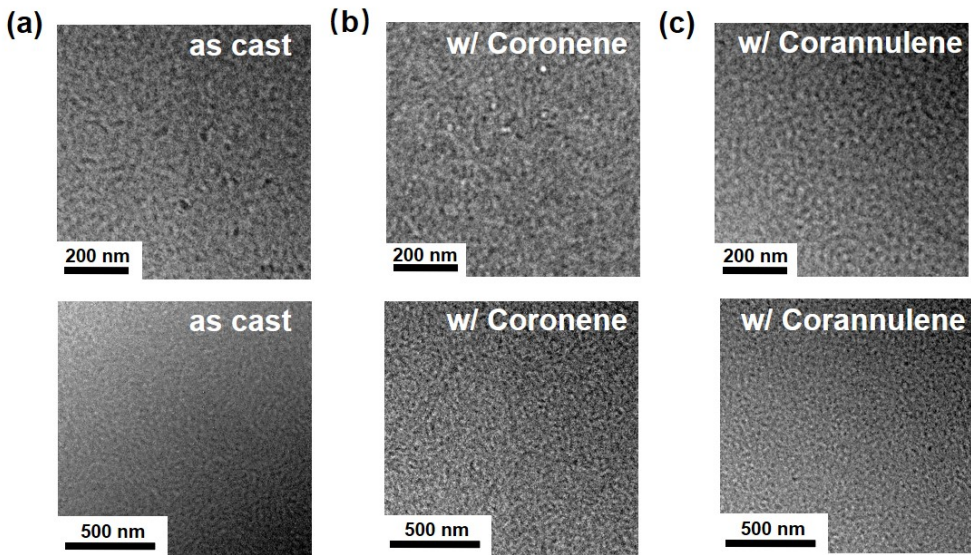


Fig. S20 TEM photographs of the blend films treated with polycyclic aromatic-based additives after TA.

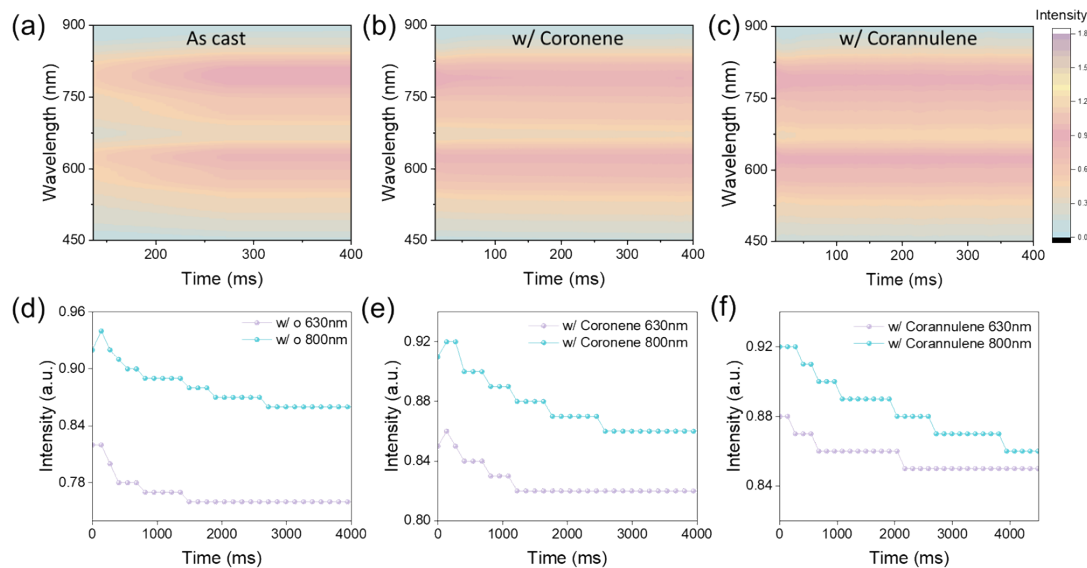


Fig. S21 *In situ* UV-vis absorption color maps and peak intensities of (a, d) pristine PM6:L8-BO, (b, e) PM6:L8-BO treated with coronene and (c, f) PM6:L8-BO treated with corannulene during thermal annealing.

3. Supplementary Tables

Table S1. DFT-calculated Gibbs free energies for the optimized configurations of PM6, L8-BO, Coronene and Corannulene.

Sample	Optimal energy (Kcal/mol)	ΔG° (Kcal/mol)
PM6	-11089.0407871	-11087.556969
L8-BO	-5290.5853728	-5289.808032
Coronene	-921.9515033	-921.711049
Corannulene	-768.1921274	-767.996877

Table S2. Calculated optimal energies and Gibbs free energies of formation for the most stable molecular conformations of PM6:Coronene and PM6:Corannulene complexes, along with the energy of the interacting molecules in the complex-forming conformation.

System	Complex	Interacting molecules		
		PM6	Solid additive	
			Optimal energy (Kcal/mol)	ΔG_f^o (Kcal/mol)
PM6:Coronene-1	-12011.0440	-12009.2910	-11089.0389	-921.9513
PM6:Coronene-2	-12011.0432	-12009.2928	-11089.0388	-921.9511
PM6:Coronene-3	-12011.0441	-12009.2929	-11089.0363	-921.9512
PM6:Coronene-4	-12011.0455	-12009.2933	-11089.0381	-921.9513
PM6:Corannuleneconc-1	-11857.2728	-11855.5700	-11089.0382	-768.1917
PM6:Corannuleneconc-2	-11857.2755	-11855.5703	-11089.0399	-768.1920
PM6:Corannuleneconc-3	-11857.2769	-11855.5705	-11089.0368	-768.1917
PM6:Corannuleneconc-4	-11857.2743	-11855.5703	-11089.0401	-768.1919
PM6:Corannuleneconv-1	-11857.2706	-11855.5672	-11089.0367	-768.9192
PM6:Corannuleneconv-2	-11857.2733	-11855.5701	-11089.0375	-768.1916
PM6:Corannuleneconv-3	-11857.2715	-11855.5665	-11089.0357	-768.1917
PM6:Corannuleneconv-4	-11857.2763	-11855.5695	-11089.0375	-768.1919

Table S3. DFT-calculated Gibbs free energies of formation, interaction energies, and reorganization energies for the complexes of PM6:Coronene, PM6:Corannulene-concave, and PM6:Corann-convex.

System	Intermolecular interaction			
	PM6 & Soild additive			
	ΔG_f° (Kcal/mol)	E_{bonding} (Kcal/mol)	$E_{\text{interaction}}$ (Kcal/mol)	$E_{\text{reorganization}}$ (Kcal/mol)
PM6:Coronene-1	-14.42	-32.47	-33.79	1.32
PM6:Coronene-2	-15.57	-31.97	-33.51	1.55
PM6:Coronene-3	-15.61	-32.5	-35.48	2.98
PM6:Coronene-4	-15.84	-33.42	-35.23	1.81
PM6:Corannuleneconc-1	-10.11	-25.05	-26.95	1.9
PM6:Corannuleneconc-2	-10.32	-26.73	-27.43	0.69
PM6:Corannuleneconc-3	-10.47	-27.62	-30.39	2.77
PM6:Corannuleneconc-4	-10.33	-25.95	-26.51	0.56
PM6:Corannuleneconv-1	-8.37	-23.65	-26.33	2.68
PM6:Corannuleneconv-2	-10.18	-25.34	-27.76	2.42
PM6:Corannuleneconv-3	-7.93	-24.19	-27.61	3.42
PM6:Corannuleneconv-4	-9.84	-27.25	-29.47	2.22

Table S4. Calculated optimal energies and Gibbs free energies of formation for the most stable molecular conformations of L8-BO:Coronene and L8-BO:Corannulene complexes, along with the energy of the interacting molecules in the complex-forming conformation.

System	Complex		Interacting molecules	
	Optimal energy (Kcal/mol)	ΔG_f° (Kcal/mol)	L8-BO	Solid additive
L8-BO:Coronene-1	-6212.5817	-6211.5404	-5290.5844	-921.9510
L8-BO:Coronene-2	-6212.5894	-6211.5473	-5290.5810	-921.9508
L8-BO:Coronene-3	-6212.5881	-6211.5461	-5290.5830	-921.9510
L8-BO:Corannuleneconc-1	-6058.8162	-6057.8210	-5290.5849	-768.1918
L8-BO:Corannuleneconc-2	-6058.8223	-6057.8243	-5290.5846	-768.1919
L8-BO:Corannuleneconc-3	-6058.8264	-6057.8287	-5290.5832	-768.1918
L8-BO:Corannuleneconv-1	-6058.8176	-6057.8237	-5290.5819	-768.1919
L8-BO:Corannuleneconv-2	-6058.8176	-6057.8237	-5290.5819	-768.1919
L8-BO:Corannuleneconv-3	-6058.8209	-6057.8274	-5290.5809	-768.1914

Table S5. DFT-calculated Gibbs free energies of formation, interaction energies, and reorganization energies for the complexes of L8-BO:Coronene, L8-BO:Corannulene-concave, and L8-BO:Corann-convex.

System	Intermolecular interaction			
	L8-BO & Soild additive			
	ΔG_f^o (Kcal/mol)	E_{bonding} (Kcal/mol)	$E_{\text{interaction}}$ (Kcal/mol)	$E_{\text{reorganization}}$ (Kcal/mol)
L8-BO:Coronene-1	-13.41	-28.16	-29.08	0.92
L8-BO:Coronene-2	-17.71	-32.95	-36.18	3.23
L8-BO:Coronene-3	-16.97	-32.17	-33.96	1.79
L8-BO:Corannuleneconc-1	-10.09	-24.27	-24.72	0.45
L8-BO:Corannuleneconc-2	-12.18	-28.11	-28.76	0.65
L8-BO:Corannuleneconc-3	-14.91	-30.68	-32.21	1.53
L8-BO:Corannuleneconv-1	-11.77	-25.13	-27.43	2.30
L8-BO:Corannuleneconv-2	-11.78	-25.13	-27.43	2.30
L8-BO:Corannuleneconv-3	-14.01	-27.25	-30.49	3.24

Table S6. Investigations of the contact angles, surface energy and interfacial tension values of PM6, L8-BO, and their corresponding blends with solid additives.

Samples	Contact		Surface Energy [mJ m ⁻²]	Relative χ^a
	Water	Ethylene glycol		
PM6	110.4°	79.3°	30.50	—
L8-BO	96.7°	65.8°	32.13	0.021 <i>K</i>
L8-BO:Coronene	97.3°	65.0°	34.26	0.109 <i>K</i>
L8-BO:Corannulene	91.7°	61.5°	31.89	0.015 <i>K</i>
PM6:Coronene	105.8°	78.1°	25.58	0.372 <i>K</i>
PM6:Corannulene	105.6°	77.6°	26.09	0.314 <i>K</i>

$\chi^a = K(\sqrt{\gamma_1} - (\sqrt{\gamma_2})^2$, where γ is the surface tension and *K* is a constant.

Table S7. Photovoltaic performance parameters of the PM6:L8-BO-based OSCs processed with different weight ratios of corannulene additive relative to the total mass of the donor material.

Weight ratio (%)	V_{oc} (V)	J_{sc} (mA cm ⁻²)	FF (%)	PCE (%)
5	0.886	27.76	80.16	19.72
10	0.889	27.72	79.49	19.59
15	0.889	27.73	80.65	19.88
20	0.893	27.01	80.61	19.44
30	0.885	26.95	80.95	19.31
40	0.885	26.82	80.57	19.12

Table S8. Photovoltaic performance parameters of PM6:L8-BO-based OSCs with 15% corannulene (relative to PM6) as the additive, treated by thermal annealing at different temperatures for 10 min, under AM 1.5 G illumination at 100 mW cm⁻².

Treatment temperature (°C)	V _{oc} (V)	J _{sc} (mA cm ⁻²)	FF (%)	PCE (%)
60	0.896	27.66	81.52	20.21
65	0.897	28.16	81.24	20.52
70	0.897	27.39	81.48	20.02
80	0.892	27.98	81.63	20.39
100	0.893	27.88	79.89	19.90

Table S9. Photovoltaic performance parameters of the PM6:L8-BO-based OSCs processed with different weight ratios of coronene additive relative to the total mass of the donor material.

Weight ratio (%)	V _{oc} (V)	J _{sc} (mA cm ⁻²)	FF (%)	PCE (%)
0	0.877	26.76	77.80	18.26
5	0.867	23.04	71.44	14.26
10	0.869	23.24	71.80	14.50
15	0.865	22.59	70.23	13.72
20	0.861	22.38	63.86	12.27

Table S10. Summary of photovoltaic device parameters of solid additive-processed OSCs.

System	Additives	V_{oc}	J_{sc} (mA cm⁻²)	FF (%)	PCE (%)	Ref
D18:L8-BO	DFBB	0.925	26.2	81.5	19.8	9
D18:L8-BO:PY-C11	HBT-2	0.91	27.41	80.23	20.01	10
D18-Cl:L8-BO	TTz-Pt	0.929	26.61	79.4	19.63	11
PM6:Y6	PAT	0.837	28.28	80.5	19.04	12
D18:L8-BO	VCB	0.91	26.43	80.35	19.33	13
PM6:L8-BO	DBrTz	0.887	27.4	79.9	19.4	14
PM6:BTP-ec9	CB-NH2	0.87	28.09	79.73	19.48	15
PM6:PY-DT	4-BDBTP	0.951	25.85	78.5	19.3	16
PM6:Y6	DPB	0.836	27.42	76.1	17.45	17
PM6:BTP-eC9-4F:DM-F	TZ-3Cl	0.902	28.01	79.83	20.2	18
D18:L8-BO	TCT	0.925	26.5	79.55	19.50	19
D18:BTP-eC9	D1-Cl	0.872	28.08	79.3	19.39	20
PM6:Y6	T5	0.84	28.35	79.31	18.89	21
PM6:PY-DT:L8-BO	SF-2	0.961	26.5	74.5	19.02	22
PM6:PY-DT-X	2-EN	0.953	25.87	79.1	19.5	23
PM6:Y6-HU	DBrDIB	0.87	27.2	80.4	19.1	24
PTVT-T:BTP-ec9	BT	0.87	27.2	80.4	19.1	25
PM6:BTP-ec9	DBE	0.86	28	80.5	19.4	26
D18-Cl:PM6:L8-BO	M1	0.924	26.95	79.1	19.7	27
PM6:BO-4Cl	MT	0.853	28.35	77.76	18.52	28
PM6:L8-BO	DIMCH	0.906	26.35	78.9	18.8	29
PM6:L8-BO	DTH	0.871	27.44	79.78	19.07	30
PM6:Y6	DFB	0.841	26.68	76.41	17.15	31
PM6:L8-BO:BTP-eC9	Th-ClSi	0.886	27.22	79.5	19.17	32
PM6 : BTP-eC9 : L8-BO	FPA	0.884	26.96	80.45	19.2	33
PM6:CH23	TT-Cl	0.879	26.73	79.68	18.72	34
D18-Cl:N3	DMNA	0.873	27.74	76.84	18.61	35
PM6:BTP-ec9	MT-I	0.852	28.58	76.29	18.59	36
PM6:Y6	EC	0.837	27.81	74.42	17.4	37
PM6:PY-IT	SL-1	0.935	26.1	78.6	19.19	38
D18-L8-BO	CBB	0.887	26.32	79.59	18.58	39

PM6:Y6-HU	DBrB	0.87	27	79	18.6	40
PM6/L8-BO	BDCB	0.891	26.8	79.7	19.03	41
D18+/L8-BO+	FeCl3	0.911	26.72	78.65	19.17	42
PM6 : L8-BO : BTP-eC9	SA1	0.873	28.07	81.6	20	43
PM6 with 10% INB-1Br/L8-BO	INB-Br	0.883	27.3	80.7	19.4	44
D18:L8-BO	DBM	0.883	27.3	80.6	19.4	45
PM6:L8-BO:BTP-eC9	DBF	0.881	27.42	79.08	19.11	46
D18-Cl:N3	CFIB	0.848	27.53	79.4	18.54	47
PM6:Y6	CBX5	0.854	26.6	71	16.1	48
D18:L8-BO	BCN	0.924	25.56	77.08	18.2	49
PM6:Y6	IC-BDTBr	0.848	26.62	73.13	16.6	50
PM6:Y6	PID	0.83	25.5	74	15.8	51
PM6:BTP-ec9	BIB	0.867	27.89	78.21	18.91	52
PTQ10:m-BTP-PhC6	CNPz	0.884	27.2	81.8	19.67	53
PM6: PM1: L8-BO	DTL	0.906	27.21	77.55	19.11	54
D18:L8-BO:BTP-eC9	p-BrCN	0.886	27.93	0.795	19.68	55
PM6:Y6	IDT	0.84	26.78	71.43	16.08	56
PM6:L8-BO	SA-T5	0.879	26.65	80.3	18.8	57
PM6:BTP-ec9	BNS-H1	0.848	27.7	79.8	18.8	58
D18-Cl: N3	TeCB	0.844	27.79	78.6	18.44	59
D18:L8-BO	CBN	0.908	26.45	79.94	19.2	60
PM6 : L8-BO	PyMC5	0.904	27.25	79.1	19.52	61
PM6 : PY-IT	SA-T1	0.933	25.61	76.5	18.3	62
PM6:Y6	2-T	0.854	26.9	78.6	18.1	63
PBTz-F:PM6:L8-BO	SIB	0.907	27.1	80.06	19.68	64
D18(TTBB)/L8-BO(TTBI)	TTBB/TT BI	0.919	27.2	79.8	19.9	65
PM6:Y6	DHT	0.859	26.64	78.38	17.93	66
D18:L8-BO	pClPA	0.903	26.02	81.01	19.04	67

Table S11. Normalized photovoltaic parameters of optimized OSCs based on DIO-processed PM6:L8-BO active layer in nitrogen atmosphere for over 600 h storage under 65°C heated conditions.

Time (h)	V _{oc} (V)	J _{sc} (mA cm ⁻²)	FF (%)	PCE (%)
0	100.00	100.00	100.00	100.00
2	99.69	94.52	99.27	93.54
4	99.65	94.31	97.69	91.81
8	99.63	92.46	97.38	89.71
16	99.65	90.87	97.49	88.27
24	98.98	90.32	98.08	87.68
30	100.24	91.45	95.35	87.40
40	98.72	90.97	94.77	85.12
52	98.76	89.99	95.36	84.75
62	98.65	90.17	94.30	83.88
80	98.11	88.60	94.99	82.57
104	98.88	88.34	93.34	81.54
130	98.88	86.81	93.13	79.94
158	98.88	85.50	93.11	78.71
184	98.56	85.79	92.58	78.28
210	97.53	85.63	93.06	77.72
240	98.08	84.78	92.16	76.64
244	97.92	85.12	91.74	76.47
264	98.88	83.04	92.02	75.55
294	97.94	83.88	90.73	74.54
344	98.19	82.81	90.73	73.77
394	98.20	80.96	89.91	71.48
466	97.66	81.22	83.24	66.02
538	96.00	79.09	81.05	61.54
610	96.09	80.36	77.68	59.99

Table S12. Normalized photovoltaic performance parameters of optimized OSCs based on coronene-processed PM6:L8-BO active layer stored under nitrogen atmosphere for over 600 h at 65°C heated conditions.

Time (h)	V _{oc} (V)	J _{sc} (mA cm ⁻²)	FF (%)	PCE (%)
0	100.00	100.00	100.00	100.00
2	97.23	99.30	91.07	87.93
4	96.92	94.83	92.16	84.71
8	98.20	95.31	89.68	83.94
16	98.75	92.91	91.38	83.83
24	98.14	92.24	91.13	82.50
30	97.86	94.68	88.57	82.05
40	97.55	94.79	88.40	81.75
52	97.21	94.54	88.12	80.99
62	97.35	93.44	88.47	80.48
80	98.11	90.82	88.77	79.10
104	99.13	91.10	87.01	78.58
130	98.07	88.09	89.26	77.10
158	96.97	91.04	86.41	76.28
184	98.01	88.06	87.20	75.26
210	98.18	86.10	88.00	74.39
240	97.80	85.77	87.32	73.25
244	94.60	87.00	86.05	70.82
264	98.88	85.84	83.18	70.60
294	98.55	84.74	84.37	70.46
344	98.53	83.32	83.23	68.32
394	98.10	83.10	77.55	63.22
466	89.31	82.79	71.26	52.69
538	92.23	81.74	64.11	48.33
610	92.57	80.87	62.09	46.48

Table S13. Normalized photovoltaic performance parameters of optimized OSCs based on corannulene-processed PM6:L8-BO active layer stored under nitrogen atmosphere for over 1500 h at 65°C heated conditions.

Time (h)	V _{oc} (V)	J _{sc} (mA cm ⁻²)	FF (%)	PCE (%)
0	100.00	100.00	100.00	100.00
2	99.84	100.27	99.84	99.95
4	99.18	100.66	100.05	99.89
8	100.31	101.39	98.16	99.83
16	100.75	100.18	98.60	99.52
24	100.37	99.65	99.46	99.48
30	100.96	99.17	99.13	99.26
40	100.84	99.35	98.61	98.79
52	100.65	98.83	98.99	98.48
62	100.46	100.50	97.32	98.25
80	100.64	99.31	98.25	98.20
104	100.53	97.91	99.27	97.71
130	100.05	98.06	99.50	97.62
158	100.32	97.53	99.37	97.23
184	100.16	97.74	98.43	96.36
210	99.34	98.36	97.63	95.39
240	98.82	98.74	96.94	94.59
244	100.08	96.38	97.83	94.36
264	98.62	96.58	99.01	94.30
294	99.77	96.50	97.82	94.18
344	99.91	95.15	98.28	93.42
394	100.01	94.39	98.57	93.05
466	100.10	96.14	95.39	91.81
538	100.71	96.25	93.57	90.70
610	100.11	94.18	95.13	89.69
682	100.35	93.30	95.43	89.34
754	99.33	93.77	95.07	88.55
826	100.41	93.75	93.76	88.26
898	99.83	93.47	93.68	87.42
970	99.95	93.65	92.44	86.53
1042	99.38	92.15	94.10	86.17
1114	99.60	93.39	92.57	86.11
1186	99.82	92.00	93.43	85.81
1258	99.21	91.95	93.91	85.67

1330	99.38	92.16	93.42	85.56
1402	99.68	93.30	91.98	85.55
1474	99.22	92.19	93.54	85.56
1574	99.38	91.39	94.42	85.49
1674	99.29	92.28	93.27	85.46
1774	98.97	93.16	92.59	85.37
1874	99.0	93.12	92.36	85.15
2042	99.68	91.96	92.69	84.96

Table S14. Summary of hole (μ_h) and electron (μ_e) mobilities treated under different conditions.

Active Layer	μ_h ($\times 10^{-4}$ cm 2 V $^{-1}$ s $^{-1}$) ^a	μ_e ($\times 10^{-4}$ cm 2 V $^{-1}$ s $^{-1}$) ^a	μ_h/μ_e
as cast	3.56	4.32	0.82
w/ Coronene	1.36	2.54	0.54
w/ Corannulene	5.22	5.72	0.91

^a Average values with standard deviation were obtained from 10 devices.

Table S15. Parameters of exciton dissociation and charge collection efficiency for PM6:L8-BO systems with different additives.

Active Layer	J_{ph} (mA cm $^{-2}$) ^a	J_{ph} (mA cm $^{-2}$) ^b	J_{sat} (mA cm $^{-2}$)	P_{diss} (%)	P_{coll} (%)
as cast	26.77	24.54	27.71	96.6	81.5
w/ Coronene	22.47	19.29	23.67	94.9	72.3
w/ Corannulene	27.79	25.28	27.89	99.6	94.5

^a Under short circuit condition. ^b Under the maximal power output condition.

Table S16. Exciton dissociation kinetics for PM6:L8-BO active layers processed without or with coronene and corannulene solid additives.

Active Layer	A1	A2	τ_1 (ps)	τ_2 (ns)	τ_{ave} (ns)
as cast	1306.381	9.562	0.225	4.515	0.256
w/ Coronene	1292.168	4.980	0.235	4.361	0.250
w/ Corannulene	1395.902	7.705	0.238	3.817	0.257

Table S17. Summary of OOP (010) coherence lengths of the neat films: L8-BO, Coronene - treated L8-BO and corannulene-treated L8-BO.

Active Layer	$d_{(010)}^{\text{OOP}}$ (\AA^{-1})	$L_{C(010)}^{\text{OOP}}$ (nm)
L8-BO	3.67	2.56
L8-BO:Coronene	3.56	1.87
L8-BO:Corannulene	3.65	3.40

Table S18. Summary of IP (100) and OOP (010) coherence lengths of the blend films: PM6:L8-BO, PM6:L8-BO with coronene and PM6:L8-BO with corannulene.

Active Layer	$d_{(100)}^{\text{IP}}$ (\AA^{-1})	$L_{C(100)}^{\text{IP}}$ (nm)	$d_{(010)}^{\text{OOP}}$ (\AA^{-1})	$L_{C(010)}^{\text{OOP}}$ (nm)
as cast	20.87	11.74	3.72	3.34
w/ Coronene	20.48	9.43	3.75	2.92
w/ Corannulene	19.02	10.29	3.70	3.72

4. Supplementary References

- [1] Gaussian 16, Revision A.03, M. J. Frisch, G. W. Trucks, H. B. Schlegel, G. E. Scuseria, M. A. Robb, J. R. Cheeseman, G. Scalmani, V. Barone, G. A. Petersson, H. Nakatsuji, X. Li, M. Caricato, A. V. Marenich, J. Bloino, B. G. Janesko, R. Gomperts, B. Mennucci, H. P. Hratchian, J. V. Ortiz, A. F. Izmaylov, J. L. Sonnenberg, D. Williams-Young, F. Ding, F. Lipparini, F. Egidi, J. Goings, B. Peng, A. Petrone, T. Henderson, D. Ranasinghe, V. G. Zakrzewski, J. Gao, N. Rega, G. Zheng, W. Liang, M. Hada, M. Ehara, K. Toyota, R. Fukuda, J. Hasegawa, M. Ishida, T. Nakajima, Y. Honda, O. Kitao, H. Nakai, T. Vreven, K. Throssell, J. A. Montgomery, Jr., J. E. Peralta, F. Ogliaro, M. J. Bearpark, J. J. Heyd, E. N. Brothers, K. N. Kudin, V. N. Staroverov, T. A. Keith, R. Kobayashi, J. Normand, K. Raghavachari, A. P. Rendell, J. C. Burant, S. S. Iyengar, J. Tomasi, M. Cossi, J. M. Millam, M. Klene, C. Adamo, R. Cammi, J. W. Ochterski, R. L. Martin, K. Morokuma, O. Farkas, J. B. Foresman, and D. J. Fox, Gaussian, Inc., Wallingford CT, 2016.
- [2] Becke, A. Assessment of a long-range corrected hybrid functional. *J. Chem. Phys.* 1993, **98**, 5648-5652.
- [3] Q. Tan, C. Shu, J. Abbott, Q. Zhao, L. Liu, T. Qu, Y. Chen, H. Zhu, Y. Liu, G. Wu, *ACS Catal.* 2019, **9**, 6362.
- [4] J. Zhang, M. Dolg, *Phys. Chem. Chem. Phys.* 2015, **17**, 24173.
- [5] J. Zhang, M. Dolg, *Phys. Chem. Chem. Phys.* 2016, **18**, 3003.
- [6] L. Liu, F. Yu, L. Du, Z. Yang, J. S. Francisco, X. Zhang, *Proc. Natl. Acad. Sci.* 2021, **118**, e2108384118.
- [7] S. Grimme, S. Ehrlich, L. Goerigk, *J. Comput. Chem.* 2011, **32**, 1456.
- [8] H. Zheng, Y. Sang, K. N. Houk, X.-S. Xue, J.-P. Cheng, *J. Am. Chem. Soc.* 2019, **141**, 16046.
- [9] W. Xiong, Y. Cui, Z. Zhang, S. Zhu, Z. Wang, Z. Chai, H. Hu, Y. Chen, *Angew. Chem. Int. Ed.* 2025, DOI:10.1002/anie.202500085.
- [10] S. Wang, S. Wang, J. Wang, N. Yu, J. Qiao, X. Xie, C. Li, M. S. Abbasi, R. Ding, X. Zhang, Y. Han, G. Lu, J. Zhang, X. Hao, Z. Tang, Y. Cai, H. Huang, *Adv. Energy Mater.* 2025, DOI:10.1002/aenm.202405205.
- [11] W. Zou, Y. Sun, L. Sun, X. Wang, C. Gao, D. Jiang, J. Yu, G. Zhang, H. Yin, R. Yang, H. Zhu, H. Chen, K. Gao, *Adv. Mater.* 2025, **37**, 2413125.
- [12] H. Fan, H. Yang, Y. Wu, C. Cui, Y. Li, *Adv. Energy Mater.* 2025, DOI: 10.1002/aenm.202405257.
- [13] Z. Xia, C. Gao, Z. Xie, M. Wu, H. Chen, T. Li, J. Zhou, T. Cai, H. Hu, J. Shuai, C. Xie, G. Zhang, W. Chen, S. Liu, *Angew. Chem. Int. Ed.* 2025, DOI:10.1002/anie.202421953.
- [14] Q. Zhang, H. Gao, L. Li, Y. Shen, M. Zuo, G. Lu, X. Wu, Y. Han, *Adv. Energy Mater.* DOI:10.1002/aenm.202404507.
- [15] H. Wang, Z. Zhong, S. Gámez-Valenzuela, J. Lee, B. Li, C. Xu, J. Yang, H. Sun, B. J. Kim, B. Liu, X. Guo, *Adv. Funct. Mater.* DOI:10.1002/adfm.202418805.
- [16] H. Ma, J. Song, J. Qiao, B. Han, Q. Wang, M. H. Jee, L. Bu, D. Wei, H. Y. Woo, X. Hao, Y. Sun, *Energy Environ. Sci.* 2025, **18**, 397.

- [17] L. Wu, M. Yun, J. Qin, S. Huang, Z. Ou, Q. Li, X. Wang, W. Yuan, L. Dong, X. Cheng, Y. Yang, Y. Zheng, K. Sun, Z. Zhang, Z. Hu, Z. Liu, Y. Leng, J. Du, *Small* 2024, **20**, 2408610.
- [18] N. Wei, H. Lu, Y. Wei, Y. Guo, H. Song, J. Chen, Z. Yang, Y. Cheng, Z. Bian, W. Zhang, Q. Chen, Y. Liu, W. Zhao, X. Xu, Z. Bo, *Energy Environ. Sci.* 2025, **18**, 2298.
- [19] Y. Cheng, H. Li, X. Zhang, Y. Chen, G. Ran, Y. Yue, N. Wei, X. Zhu, X. Yan, Y. Liu, H. Lu, Y. Liu, Y. Wei, W. Zhang, Z. Bo, *Adv. Funct. Mater.* 2025, **35**, 2415468.
- [20] W. Su, X. Zhou, Q. Wu, Y. Wu, H. Qin, Z. Liang, H. Li, H. Bai, J. Guo, L. Jiang, Y. Liu, R. Ma, Y. Li, W. Zhu, Q. Fan, *Adv. Funct. Mater.* 2025, **35**, 2415090.
- [21] Z. Li, L. Zhan, H. Qiu, X. Sun, H. Hu, R. Gui, H. Yin, R. Sun, J. Min, J. Yu, W. Fu, W. Qiu, Z.-X. Liu, S. Yin, H. Chen, *Energy Environ. Sci.* 2024, **17**, 8293.
- [22] T. Chen, Y. Zhong, T. Duan, X. Tang, W. Zhao, J. Wang, G. Lu, G. Long, J. Zhang, K. Han, X. Wan, B. Kan, Y. Chen, *Angew. Chem. Int. Ed.* 2025, **64**, e202412983.
- [23] J. Song, C. Li, H. Ma, B. Han, Q. Wang, X. Wang, D. Wei, L. Bu, R. Yang, H. Yan, Y. Sun, *Adv. Mater.* 2024, **36**, 2406922.
- [24] M. Haris, Z. Ullah, S. Lee, D. H. Ryu, S. U. Ryu, B. J. Kang, N. J. Jeon, B. J. Kim, T. Park, W. S. Shin, C. E. Song, *Adv. Energy Mater.* 2024, **14**, 2401597.
- [25] B. Liu, S. Gámez-Valenzuela, J.-W. Lee, B. Li, W. Yang, K. Wang, Z. Zhong, J. Yang, Z. Wang, C. Xu, H. Sun, B. J. Kim, X. Guo, *ACS Energy Lett.* 2024, **9**, 3727.
- [26] S. Gao, Y. Zhang, S. Jeong, X. Zhou, H. Xu, S. Xu, D. Chen, W. Liu, C. Yang, S. Meng, W. Zhu, X. Song, *Energy Environ. Sci.* 2024, **17**, 5542.
- [27] Y. Miao, Y. Sun, W. Zou, X. Zhang, Y. Kan, W. Zhang, X. Jiang, X. Wang, R. Yang, X. Hao, L. Geng, H. Xu, K. Gao, *Adv. Mater.* 2024, **36**, 2406623.
- [28] Z. Jia, J. Pan, X. Chen, Y. Li, T. Liu, H. Zhu, J. Yao, B. Yan, Y. (Michael) Yang, *Energy Environ. Sci.* 2024, **17**, 3908.
- [29] H. Xiang, F. Sun, X. Zheng, B. Gao, P. Zhu, T. Cong, Y. Li, X. Wang, R. Yang, *Adv. Sci.* 2024, **11**, 2401330.
- [30] Z. Zhang, Q. Chen, C. Zhang, W. L. Tan, G. Zhang, Z. Bu, C. Xiao, X. Shen, Z. Tang, C. R. McNeill, W. Li, *Adv. Funct. Mater.* 2024, **34**, 2401823.
- [31] J. Xie, J. Deng, Y. Pei, S. Y. Jeong, B. Huang, D. Zhou, H. Y. Woo, J. Xu, F. Wu, L. Chen, *Adv. Funct. Mater.* 2024, **34**, 2402281.
- [32] W. Su, X. Zhou, Z. Yao, H. Bai, Y. Duan, R. Sun, Y. Wu, Q. Wu, H. Qin, C. Zhao, W. Zhu, H. Y. Woo, J. Min, Y. Li, W. Ma, Q. Fan, *Adv. Funct. Mater.* 2024, **34**, 2313744.
- [33] R. Yu, R. Shi, Z. He, T. Zhang, S. Li, Q. Lv, S. Sha, C. Yang, J. Hou, Z. Tan, *Angew. Chem.* 2023, **135**, e202308367.
- [34] X. Cao, J. Guo, Z. Li, X. Bi, H. Liang, Z. Xiao, Y. Guo, X. Jia, Z. Xu, K. Ma, Z. Yao, B. Kan, X. Wan, C. Li, Y. Chen, *ACS Energy Lett.* 2023, **8**, 3494.
- [35] Y. Liu, S.-Q. Ye, H.-J. Deng, L. Chen, Z.-C. Yin, Z. Xu, Y.-X. Lei, Q. Zhang, S. Yang, G.-W. Wang, *ACS Appl. Energy Mater.* 2025, **8**, 1387.
- [36] X. Jiang, P. Huang, K. Tu, L. Liu, C. Chen, Y. Li, H. Lei, F. Yu, K. Yang, Y. Chen, H. Chen, Z. Shen, H. Li, D. Hu, T. Duan, Z. Xiao, *Small* 2025, **21**, 2410470.
- [37] Z. Suo, X. Si, W. Zhao, L. Li, J. Liu, J. Wang, Z. Yao, G. Long, C. Li, X. Wan, Y. Chen, *Sol. RRL* 2025, DOI:10.1002/solr.202400927.

- [38] Q. Liang, H. Li, W. Xu, J. Lu, R. Ma, Q. Bai, X. Sun, M. Chen, L. Zhu, Q. Liu, Y. Guo, G. Zhang, Q. Xue, A. Iwan, P. Cheng, H. Hu, H. Wang, J. Chen, L. Niu, H. Sun, *Angew. Chem. Int. Ed.* 2025, DOI:10.1002/anie.202421953.
- [39] L. Kong, X. Wang, M. Li, Z. Zhang, M. Chen, L. Zhang, L. Ying, D. Ma, J. Chen, *Adv. Energy Mater.* 2024, **14**, 2402517.
- [40] M. Haris, D. H. Ryu, Z. Ullah, B. J. Kang, N. J. Jeon, S. Lee, H. K. Lee, S. K. Lee, J. Lee, H. Kwon, W. S. Shin, C. E. Song, *EcoMat* 2024, **6**, e12436.
- [41] W. Wu, Y. Luo, T. A. Dela Peña, J. Yao, M. Qammar, M. Li, H. Yan, J. Wu, R. Ma, G. Li, *Adv. Energy Mater.* 2024, **14**, 2400354.
- [42] Q. Chen, Z. Bian, Y. Yang, X. Cui, C. Jeffreys, X. Xu, W. Li, Y. Liu, M. Heeney, Z. Bo, *Angew. Chem. Int. Ed.* 2024, **63**, e202405949.
- [43] Z. Ge, J. Qiao, Y. Li, J. Song, X. Duan, Z. Fu, H. Hu, R. Yang, H. Yin, X. Hao, Y. Sun, *Angew. Chem. Int. Ed.* 2025, **64**, e202413309.
- [44] Z. Chen, C. Guo, L. Wang, C. Chen, J. Cai, C. Liu, Z. Gan, Y. Sun, J. Zhou, J. Zhou, D. Liu, T. Wang, W. Li, *Small* 2024, **20**, 2401050.
- [45] C. Han, B. Cheng, Q. Guo, Z. Fu, J. Qiao, S. Cheng, Y. Huo, X. Xia, H. Wang, Y. Fu, X. Guo, X. Lu, X. Hao, Y. Li, M. Zhang, *Adv. Funct. Mater.* 2025, **35**, 2416381.
- [46] J. Xu, C. Xiao, Z. Zhang, J. Zhang, B. Wang, C. R. McNeill, W. Li, *Small* 2024, **20**, 2405573.
- [47] J. Park, S. Jeong, Z. Sun, T. L. H. Mai, S. Jeong, S. Yang, C. Yang, *Small* 2024, **20**, 2405415.
- [48] K. Wang, S. Liu, L. Zhang, S. Zhang, *Mater. Lett.* 2024, **367**, 136663.
- [49] Y. Gong, S. Li, W. Liu, S. Zhu, X. Hu, J. Yuan, L. Jiang, Y. Li, Y. Zou, *Surf. Interfaces* 2024, **51**, 104686.
- [50] R. Lin, H. Zhou, X. Xu, X. Ouyang, *Dyes Pigments* 2024, **224**, 111980.
- [51] M. Choi, H.-S. Jeong, J. Lee, Y. Choi, I.-B. Kim, D.-Y. Kim, H. Kang, S.-Y. Jang, *J. Mater. Chem. A* 2024, **12**, 8963.
- [52] Z. Mei, R. Li, K. Li, Y. Wu, Y. Chen, H. Geng, Q. Liao, C. An, H. Fu, *J. Mater. Chem. A* 2024, **12**, 28254.
- [53] L. Tu, H. Wang, W. Duan, R. Ma, T. Jia, T. A. Dela Peña, Y. Luo, J. Wu, M. Li, X. Xia, S. Wu, K. Chen, Y. Wu, Y. Huang, K. Yang, G. Li, Y. Shi, *Energy Environ. Sci.* 2024, **17**, 3365.
- [54] L. Cao, H. Zhang, J. Du, Z. He, X. Du, H. Lin, C. Zheng, G. Yang, X. Li, S. Tao, *J. Energy Chem.* 2025, **103**, 19.
- [55] H. Liu, H. Bai, Y. Zhou, P. Li, W. Su, C. Liu, X. Liao, B. Song, X. Li, Z. Bi, C. Zhao, H. Liu, G. Lu, H. Du, L. Jiang, Y. Liu, R. Ma, W. Ma, Q. Fan, *Mater. Sci. Eng. R Rep.* 2025, **162**, 100879.
- [56] V. G. Sree, T. Gokulnath, B. Yadagiri, J. I. Sohn, H.-S. Kim, C. Bathula, *Mater. Today Phys.* 2024, **47**, 101538.
- [57] T. Chen, Y. Bai, X. Ji, W. Feng, T. Duan, X. Jiang, Y. Yi, J. Yu, G. Lu, X. Wan, B. Kan, Y. Chen, *Nano Energy* 2024, **125**, 109604.
- [58] R. Hao, H. Xia, X. Wang, H. Wei, J. Huang, F. Wang, Y. Zhang, H. Tan, M. Zhu, X. Song, Q. Fan, W. Zhu, *Chem. Eng. J.* 2024, **488**, 151067.

- [59] Y. Kim, S. Kim, S. Lee, J. Park, T. L. H. Mai, S. Yang, J. Park, S. Jeong, C. Yang, *Chem. Eng. J.* 2025, **503**, 158329.
- [60] R. Lin, Z. Luo, Y. Wang, J. Wu, T. Jia, W. Zhang, X. Gu, Y. Liu, L. Xiao, Y. Min, *Chem. Eng. J.* 2025, **503**, 158635.
- [61] Y. Wang, W. Sun, Y. Zhang, B. Zhang, Y. Ding, Z. Zhang, L. Meng, K. Huang, W. Ma, H. Zhang, *Angew. Chem. Int. Ed.* 2025, **64**, e202417643.
- [62] W. Feng, T. Chen, Y. Li, T. Duan, X. Jiang, C. Zhong, Y. Zhang, J. Yu, G. Lu, X. Wan, B. Kan, Y. Chen, *Angew. Chem. Int. Ed.* 2024, **63**, e202316698.
- [63] W. Liang, L. Chen, Z. Wang, Z. Peng, L. Zhu, C. H. Kwok, H. Yu, W. Xiong, T. Li, Z. Zhang, Y. Wang, Y. Liao, G. Zhang, H. Hu, Y. Chen, *Adv. Energy Mater.* 2024, **14**, 2303661.
- [64] T. Zhou, W. Jin, Y. Li, X. Xu, Y. Duan, R. Li, L. Yu, Q. Peng, *Adv. Sci.* 2024, **11**, 2401405.
- [65] J. Zhou, C. Guo, L. Wang, C. Chen, Z. Gan, Y. Sun, C. Liu, J. Zhou, Z. Chen, D. Gao, W. Xia, D. Liu, T. Wang, W. Li, *Nano Energy* 2024, **129**, 109988.
- [66] D. Liu, H. Zhang, H. Shen, Z. Jiang, X. Liu, H. Chen, Q. Peng, J. Yang, Y. Chen, J. Ding, X. Qi, X. Gong, *Chem. Eng. J.* 2025, **508**, 161037.
- [67] S. Xia, J. Xu, Z. Wang, S. Lee, L. Wang, Y. Hu, X. Zhao, C. Yang, E. Zhou, Z. Yuan, *Angew. Chem. Int. Ed.* 2025, DOI:10.1002/ange.202501816.